

Probing dark exciton navigation through a local strain landscape in a WSe₂ monolayer

Ryan J. Gelly^{1*}, Dylan Renaud^{2*}, Xing Liao³, Benjamin Pingault², Stefan Bogdanovic², Giovanni Scuri¹, Kenji Watanabe⁴, Takashi Taniguchi⁵, Bernhard Urbaszek⁶, Hongkun Park^{1,3†}, Marko Lončar^{2†}

¹Department of Physics, ²John A. Paulson School of Engineering and Applied Sciences, and ³Department of Chemistry and Chemical Biology, Harvard University, Cambridge, MA 02138, USA

⁴Research Center for Functional Materials, and ⁵International Center for Materials Nanoarchitectonics, National Institute for Materials Science, 1-1 Namiki, Tsukuba 305-0044, Japan

⁶Université de Toulouse, INSA-CNRS-UPS, LPCNO, 135 Avenue Rangueil, 31077 Toulouse, France

*These authors contributed equally to this work

†To whom correspondence should be addressed: loncar@seas.harvard.edu and hongkun_park@harvard.edu

Received: February 18, 2021

Monolayers of transition metal dichalcogenides (TMDs) have recently emerged as a promising optoelectronic platform. To leverage their full potential, however, it is important to understand and engineer the properties of the different exciton species that exist in these monolayers, as well as to control their transport through the material. A promising approach relies on engineering strain landscapes in atomically thin semiconductors that excitons navigate. In WSe₂ monolayers, for example, localized strain has been used to control the emission wavelength of excitons, induce exciton funneling and conversion, and even realize single-photon sources & quantum dots. Before these phenomena can be fully leveraged for applications, including quantum information processing, the details of excitons' interaction with the strain landscape must be well understood. To address this, we have developed a cryogenic technique capable of probing the dynamics of both bright and dark excitons in nanoscale strain landscapes in TMDs. In our approach, a nanosculpted tapered optical fiber is used to simultaneously generate strain and probe the near-field optical response of WSe₂ monolayers at 5 K. When the monolayer is pushed by the fiber, its lowest energy photoluminescence (PL) peaks red shift by as much as 390 meV, (corresponding to 20% of the bandgap of an unstrained WSe₂ monolayer). The red-shifting peaks are polarized perpendicularly to the WSe₂ plane and have long rising times (10 ps) and lifetimes (52 ps), indicating that they originate from nominally spin-forbidden dark excitons. Taken together, these observations indicate that dark excitons are funneled to the high-strain regions during their long lifetime and are the principal participants in drift and diffusion at cryogenic temperatures. Our work elucidates the important role that dark excitons play in locally strained WSe₂. This insight supports recent proposals on the origin

of single-photon sources in these monolayers and demonstrates a route towards engineering deep exciton traps for exciton condensation in monolayer semiconductors.

WSe₂ monolayers are direct bandgap semiconductors whose optical properties are dominated by the presence of bound electron-hole pairs, namely excitons. WSe₂, a member of the larger class of semiconducting transition metal dichalcogenides (TMDs), has several attractive properties: its monolayers have an optically dark exciton ground state [1-3], can host single-photon sources[4,5], and have potential for efficient exciton funneling [6,7]. Critically, the single-photon sources and exciton funneling schemes rely on the presence of local strain landscapes that are imposed on the WSe₂ monolayer.

Previous studies on local strain effects in atomically thin semiconductors have been limited to static[4,5,8-10], low strain[6], or room-temperature [7,11] situations. Consequently, the precise effects of local strain on excitonic properties could not be studied in detail. Here, we systematically address the role of localized strain on excitonic species in WSe₂ monolayers by dynamically generating nanoscale strain at cryogenic temperatures. We use the tip of a nanosculpted tapered optical fiber to locally deform the monolayer and to optically probe the region (Fig. 1a, Supplementary Information Figure S1). By mounting the optical fiber on a piezoelectric nanopositioner, we are able to controllably and reversibly strain the suspended WSe₂ monolayer. Optical characterization is achieved by using the fiber's fundamental mode to both excite and collect emission at the fiber's facet. We engineer the fiber to have a tip radius of 240 nm to maximize the coupling efficiency of ~700 nm light while still retaining well-localized excitation and collection profiles (Fig. 1b, Supplementary Information Figure S2). We

encapsulate a WSe₂ monolayer between two layers of hexagonal boron nitride (hBN) that increase the resistance to tearing [12]. Encapsulation and suspension of WSe₂ monolayers also leads to improved, spatially homogeneous optical properties [13,14].

Figure 1c shows the fiber-collected transmittance spectrum of a proximal, strain-free hBN/WSe₂/hBN heterostructure **D1** in a cryogenic environment (T = 5 K), measured by illuminating it with white light from the backside. The spectrum shows four transmittance dips that correspond to the A and B excitons (X_{A:1s} and X_{B:1s}) [15,16] and their first excited Rydberg counterparts (X_{A:2s} and X_{B:2s}) [15,16]. Figure 1d presents a fiber-collected PL spectrum from **D1** measured by exciting through the fiber, again without an applied strain at 5 K. The PL spectrum shows a different set of four prominent peaks, originating from (in descending order in energy) the spin-allowed, neutral, bright exciton (X⁰) [15], charged exciton (X⁻) [17], nominally spin-forbidden, z-polarized, dark exciton (D⁰) [1-3], and a phonon replica of the dark exciton (D^R) [18,19]. We detect not only bright excitons whose transition dipole moment lies in the WSe₂ plane, but also dark excitons whose transition dipole moments lie out-of-plane [3] because the fiber is in close proximity with **D1** and couples to the near field (Fig. 1b, Supplementary Information Figure S2). Therefore, the strong intensity of dark excitons in Fig. 1d is a direct consequence of using a tapered optical fiber for interrogating the WSe₂ monolayer.

We now apply a controlled strain to an hBN/WSe₂/hBN heterostructure by pushing the fiber tip against it with a piezoelectric nanopositioner. We simultaneously monitor both transmission and PL spectra as a function of the voltage applied to the piezo-positioner (V_p). For device **D2**, when we apply $V_p < 1V$, the dips in the transmission and the peaks in the PL spectra red-shift with

increasing V_p (Figs. 1e and 1f, respectively). Tracking the Rydberg states of the A exciton as a function of strain reveals only a small (~ 2 meV) change in the exciton binding energy (Supplementary Information Figure S3). Thus, we attribute shifts in PL primarily to the strain-induced change in bandgap [20,21].

As we continue pushing the hBN/WSe₂/hBN heterostructure by applying larger V_p , its spectral response changes dramatically. The transmittance spectra, measured in device **D3**, plateaus as V_p increases to 10 V (Fig. 2a). The PL, on the other hand, exhibits a radically different spectrum (Fig. 2b) at $V_p = 10$ V, compared to $V_p = 0$. As shown in Fig. 2c, the PL spectrum branches abruptly into two distinct sets at around $V_p \sim 1.5$ V. The higher energy (~ 1.7 eV) set, consisting of a number of plateauing features, does not exhibit an energy shift in the V_p range of 1.5 V to 10.0 V, similar to the transmittance spectra. The lower energy (< 1.6 eV) red-shifting set, on the other hand, shifts in energy by more than 390 meV in the same V_p range, reaching 1.38 eV at $V_p = 10.0$ V. Remarkably, this energy shift corresponds to over 20% of the bandgap of an unstrained WSe₂ monolayer.

Insight into the origin of the two branches is provided by the polarization-selective PL spectra from **D3** in Figs. 3a-c that are confocally measured from the side of the heterostructure. The lower energy (< 1.6 eV), red-shifting PL peaks that appear in the high- V_p (and thus high-strain) regime are predominantly polarized out of the plane of the WSe₂ monolayer, while the higher-energy (1.7 eV), plateauing PL peaks are not z-polarized. This observation indicates that the lower energy red-shifting PL peaks stem from the out-of-plane polarized dark excitons, while the higher energy PL peaks are primarily from bright excitons [1,3]. Charge tuning measurements

provide additional evidence that dark excitons and their phonon replicas feature prominently in the red-shifted peaks on the basis of known energetic splittings and intrinsic regime widths [19,22] (Supplementary Information Figure S4).

The data in Figs. 2 and 3 demonstrate that both bright and dark excitons play important roles in determining the optoelectronic response of a WSe₂ monolayer in the presence of strain. To better understand the nature of these roles, we utilize time-resolved PL to directly probe the exciton dynamics. Using a 1 ps above-bandgap pulsed laser (400 nm) and a streak camera (2 ps resolution), we probe the integrated intensity from the red-shifted features and the plateauing features in device **D4** (Fig. 4a, associated spectrum in Supplementary Information Figure S5). The associated lifetimes are 8 ps for the plateauing features and 52 ps for the red-shifted features. The longevity of the red-shifted PL peaks compared to the plateauing counterpart is consistent with the identification of the two sets as dark and bright excitons, respectively [23]. Notably, in addition to the differing lifetimes, the two sets have different early time behaviors as well. The bright exciton population rises concurrently with the laser pulse, while the dark exciton population does not reach its peak until after a ~10 ps delay. This clearly resolvable rise time delay indicates that dark excitons in the red-shifted branch populate more slowly than excitons in the high-energy branch.

An explanation of the observed behavior is provided by considering the spatially-dependent strain profile generated by the fiber. We calculate the strain profile in a hBN/WSe₂/hBN heterostructure pushed by a flat fiber using a finite element method (Fig. 4b, see Supplementary Information Figure S6). These calculations reveal that there are two regions with qualitatively

different strain behaviors. At the fiber facet, the membrane undergoes no appreciable change in strain due to its adhesion to the silica facet [24]. In an annular region at the fiber circumference, however, the tensile strain applied to the heterostructure reaches 5% when it is displaced 300 nm by the fiber.

This strain landscape from the finite element analysis, combined with the excitation and collection profiles in Fig. 1b suggest a model that explains the excitonic behaviors of a locally strained WSe₂ monolayer. In this model, the red-shifting dark-exciton features are associated with the fiber circumference, where the strain increases with increasing displacement. The plateauing features are, on the other hand, associated with excitons at the fiber facet where strain increases minimally. Because the excitation profile is concentrated at the center of the fiber, any excitons that reach the fiber circumference must arrive via diffusion and drift, as depicted in Fig. 4c.

This model explains not only the origin of the two sets of features that we observe at high strain, but also the preponderance of dark excitons in the red-shifted features and the delay in the onset of the time-resolved PL. Drift and diffusion are not instantaneous processes, and the time it takes for the excitons to transit from the excitation site to the circumference explains the 10 ps delay. Based on the previously measured diffusivity of dark excitons [25], dark excitons are expected to diffuse 450 nm in 10 ps, roughly equivalent to the length scale in our strain landscape set by the fiber's diameter. Moreover, because this delay time is longer than the bright exciton lifetime, any bright excitons in the system will decay before reaching the circumference. Dark excitons

are the only ones that can reach the circumference, consistent with the out-of-plane polarization of the red-shifted features.

To see how our interpretation above translates to other material systems, we repeat the strain tuning measurements on an hBN/monolayer MoSe₂/hBN heterostructure. At low V_p and thus low strain, we observe a qualitatively similar behavior to a WSe₂ monolayer (see Supplementary Information Figure S7). In the case of MoSe₂ heterostructures, however, we do not observe red-shifting features even at the large V_p limit. This observation is consistent with the above interpretation because, unlike the case of a WSe₂ monolayer, the dark excitons in a MoSe₂ monolayer lie higher in energy than the bright-exciton ground state [26], making dark exciton transport across the strain landscape unobservable.

The experimental technique that we developed allowed us to locally generate and optically probe strain fields in suspended WSe₂ monolayers. Remarkably, using strain, we achieved the red-shift of dark-exciton PL peaks by as much as 390 meV, which corresponds to 20% of the bandgap of an unstrained WSe₂ monolayer. We also show that charge control is compatible with straining the device. This exceptional tunability, from the visible to the near infrared, highlights the potential of two-dimensional materials for realizing novel optoelectronic devices. Finally, we uncovered the role that dark excitons play in the transport of energy across strain landscapes. Our results support recent theoretical proposals [27] that efficient funneling of dark excitons is a key ingredient in forming single photon sources under localized strain. Our results also suggest that the scarcity of strain-induced single-photon sources in MoSe₂ monolayers may stem from the fact that the dark excitons are not the lowest energy excitonic state in that system. Finally, the

ability to create energetic traps hundreds of meV deep via strain coupled with the long lifetime of dark excitons indicate a potential route for creating dark exciton condensates in a monolayer semiconductor [28,29].

Acknowledgments

M.L. acknowledges ARO MURI grant no. W911NF1810432, STC Center for Integrated Quantum Materials, NSF grant no. DMR-1231319, and ONR MURI grant no. N00014-15-1-2761.. H.P. acknowledges support from the DoD Vannevar Bush Faculty Fellowship (N00014-16-1-2825), NSF (PHY-1506284), NSF CUA (PHY-1125846), ARL (W911NF1520067), DOE (DE-SC0020115), and Samsung Electronics. B.U. acknowledges funding from ANR 2D-vdW-Spin, ANR MagicValley and the EUR grant NanoX n° ANR-17-EURE-0009 in the framework of the Programme des Investissements d’Avenir. K.W. and T.T. acknowledge support from the Elemental Strategy Initiative conducted by the MEXT, Japan and the CREST (JPMJCR15F3), JST. D.R. acknowledges support from the NSF GRFP and Ford Foundation fellowships. B.P. acknowledges financial support through a Horizon 2020 Marie Skłodowska-Curie Actions global fellowship (COHESiV, Project Number: 840968) from the European Commission. Device fabrication was performed at the Center for Nanoscale Systems (CNS), a member of the National Nanotechnology Coordinated Infrastructure Network (NNCI), which is supported by the National Science Foundation under NSF Grant No. 1541959.

Appendix: Methods

Sample preparation

Monolayer WSe₂ & MoSe₂ (HQ Graphene) and few-layer graphite flakes were exfoliated onto silicon substrates with a 285 nm silicon oxide layer. hBN flakes were exfoliated onto silicon substrates with a 90 nm silicon oxide layer. Monolayers of WSe₂ and MoSe₂ were identified by their contrast under an optical microscope and verified by their PL spectra. Both hBN/WSe₂/hBN and hBN/WSe₂/hBN/graphite heterostructures were fabricated by a dry transfer method. These heterostructures were then transferred to glass substrates with pre-patterned pits formed by reactive ion etching (4 μm diameter, 0.5-2.0 μm deep) in order to be suspended. Next, electron-beam lithography was used to define contacts to the WSe₂ and few-layer graphite (where applicable) and deposited by thermal evaporation (5 nm chromium and 95 nm gold).

Fiber preparation and fiber-based spectroscopy

Commercial near-infrared single mode optical fibers (Thorlabs S630-HP) are stripped of their buffer coating and cleaned before being submerged in hydrofluoric acid (HF) to generate their taper profile[30]. The taper tip is then deterministically etched by mounting the tapered fiber in a focused-ion beam (FIB) microscope. Standard ionic-clean (SC-2) is subsequently carried out to remove potential residuary ions (Ga⁺) from the FIB processing.

The fiber is mounted on a stack of piezoelectric nanopositioners (Attocube) allowing for three-dimensional positioning. The heterostructures are also mounted on a stack of nanopositioners. Using a camera, the fiber and sample are aligned to each other before approach. A 520 nm CW laser with 30-500 nW of power is coupled into the fiber to excite the sample and PL is collected along the same path, using a non-polarizing beamsplitter and long-pass filter at 590nm to separate PL from reflected laser light.

Polarization-selective optical spectroscopy

With the sample and fiber mounted inside a Montana Instruments cryostat at 5 K, measurements were made through the side window using a home-built confocal microscope with a 100x, 0.9 NA objective (Olympus). The sample is excited through the fiber with 520 nm laser light and PL is collected confocally after a 715 nm long-pass filter. A half-wave plate rotates the polarization of the PL before passing through a linear polarizer.

Time-resolved photoluminescence spectroscopy

A fs-pulsed laser (Mira F-900) with a repetition rate of 79 MHz and with wavelength 800 nm is frequency-doubled to 400 nm and sent through the fiber to excite the sample. PL is collected through the same fiber and directed to a streak camera (Hamamatsu C5680 and Hamamatsu ORCA-IR) with a 2 ps resolution. A collection of tunable short-pass and long-pass filters are used to spectrally isolate certain PL features before sending them to the streak camera.

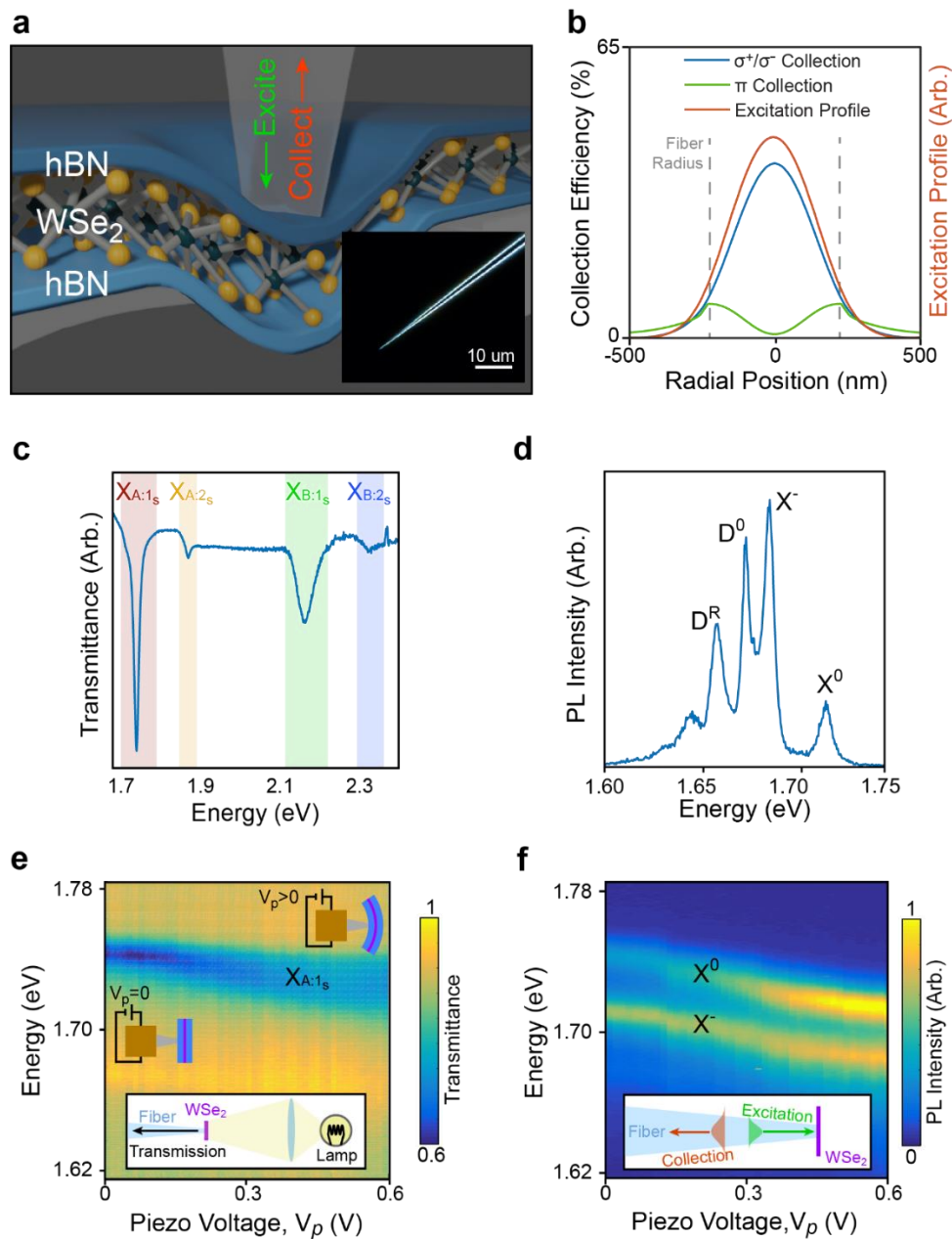


Figure 1 – A cryogenic fiber-based technique for strain-dependent spectroscopy. (a) A schematic of the fiber interfacing with an hBN/WSe₂/hBN heterostructure. The fiber is mounted on a piezoelectric nanopositioner (not pictured). Inset: Darkfield optical micrograph of a 240 nm radius tapered fiber. (b) We simulate excitation and collection profiles (for both circularly

polarized (σ^+ / σ^-) and z-polarized (π) light, for z-axis normal to the WSe₂) for a 240 nm radius fiber tip and 700 nm light. (c) White light transmitted through the device in a cryogenic environment ($T = 5$ K) and collected by the fiber (depicted schematically in inset) shows four transmittance dips. They correspond to the A and B excitons ($X_{A:1s}$, $X_{B:1s}$) and their first excited Rydberg states ($X_{A:2s}$, $X_{B:2s}$). (d) Fiber-collected PL at 5 K shows four pronounced features originating from (in decreasing energy) the neutral exciton (X^0), the charged exciton (X^-), the dark exciton (D^0), and the dark exciton's phonon replica (D^R). (e) As we push the device with the fiber by increasing the piezo-positioner voltage (V_p), we observe a decrease in the energy of the $X_{A:1s}$ transmittance dip with increased fiber displacement. (f) Likewise, for the same fiber displacement as in (e), we observe decreases in the energy of the X^0 and X^- in PL. Data in (c), (d) come from device **D1**, while data in (e), (f) come from **D2**. **D1** and **D2** vary only by few-nm differences in hBN thicknesses.

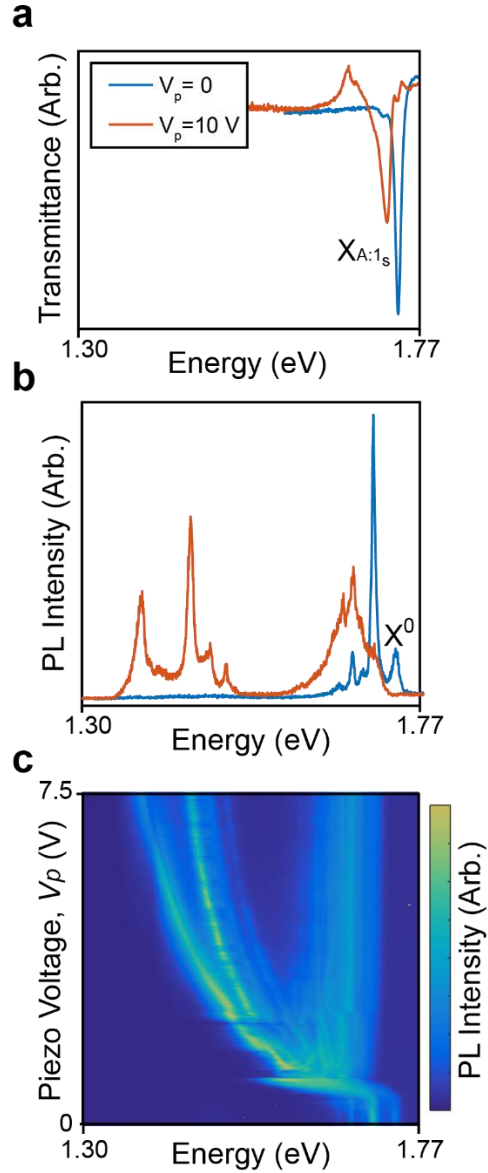


Figure 2 – Strain-induced excitonic response in transmittance and PL with large tunability at $T = 5$ K. (a) For device **D3**, we present the transmittance dip associated with $X_{A:1s}$ with $V_p = 0$ (before contacting the heterostructure with the fiber) and with $V_p = 10$ V (the maximum voltage we can apply to the piezo-positioner). The $X_{A:1s}$ feature shifts by 35 meV over this range. (b) The fiber-collected PL has a feature X^0 that matches in energy with $X_{A:1s}$ at $V_p = 0$. At $V_p = 10$ V, peaks as low as 1.38 eV appear. (c) PL spectra as a function of piezo-positioner voltage shows

two branches of features. The branch that is lower in energy shifts by 390 meV from the unstrained X^0 resonance.

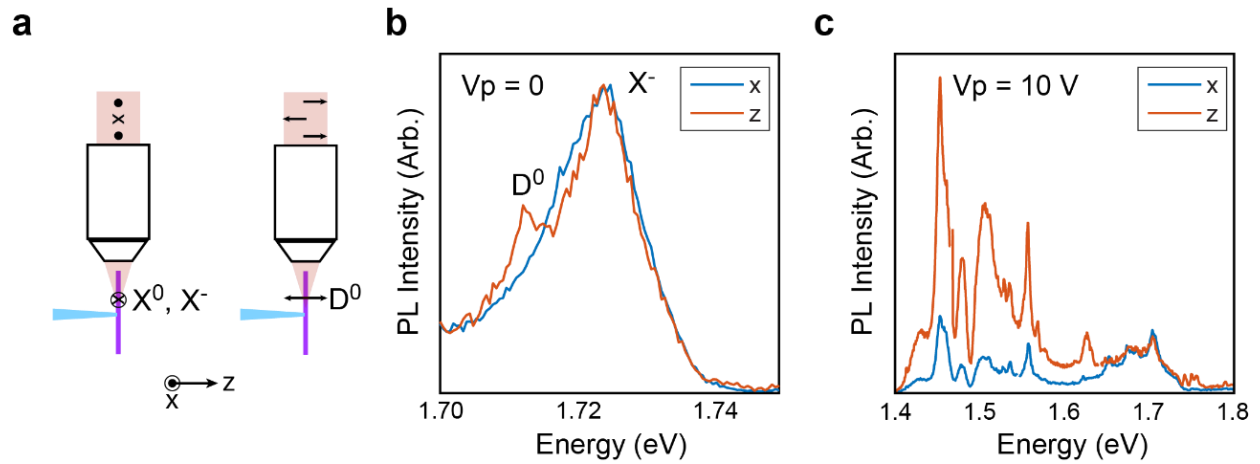


Figure 3 – Transition dipole moment measurement by polarization-selective PL

spectroscopy. (a) A scheme whereby polarization-selective, confocal collection of light from the side of the WSe₂ monolayer (purple) can distinguish between in-plane (parallel to the device) optical dipoles (such as associated with X⁰ and X⁻) and out-of-plane (perpendicular to the device) optical dipoles (such as associated with D⁰). We label in-plane polarization as x, and out-of-plane polarization as z. We use this measurement scheme to resolve the dipole moment of transitions in **D3**. (b) Before straining the sample ($V_p = 0$), X⁻ is present when selecting for x-polarized light, but D⁰ appears when selecting for z-polarized light. (c) At $V_p = 10$ V, the red-shifted features (< 1.6 eV) possess a much greater degree of z-polarization than the plateauing branch (~ 1.7 eV).

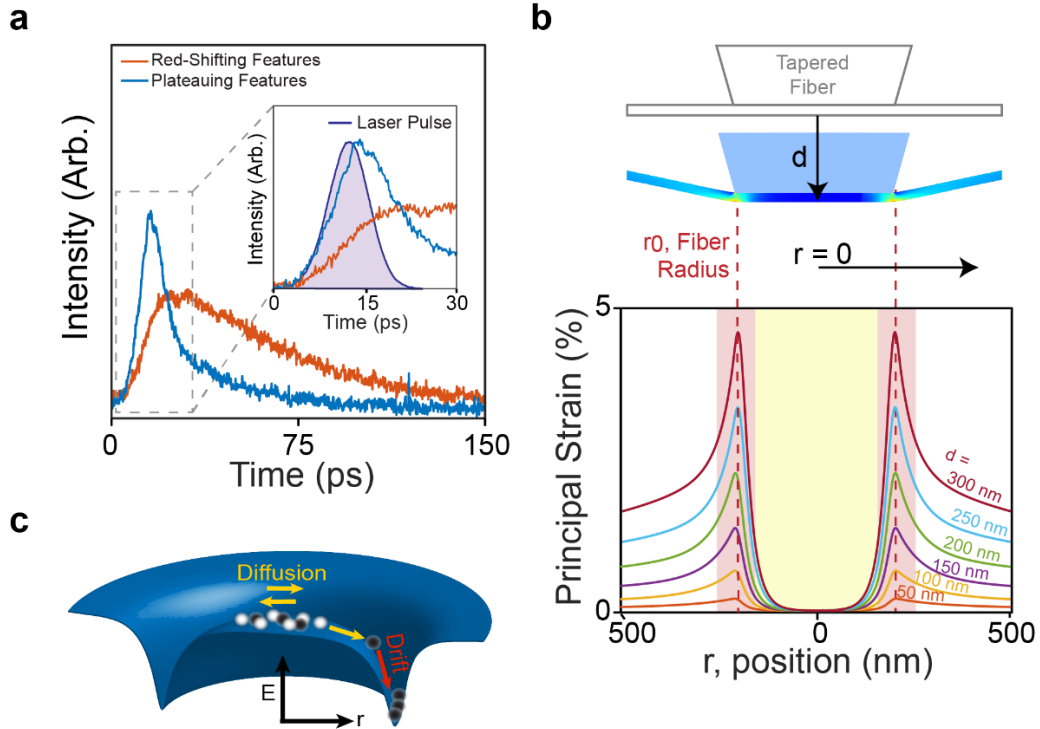


Figure 4 – Dark and bright exciton navigation across a local strain landscape. (a) Time-resolved PL from both the plateauing features and red-shifting features in device **D4** reveal lifetimes associated with each set of 5.4 ± 0.2 ps and 48.2 ± 0.6 ps respectively. Inset: Close up of the first 30 ps of the time evolution, with the laser pulse shown. The red-shifted features have a ~ 10 ps delay relative to the plateauing features. (b) Finite element method modeling of strain in the hBN/WSe₂/hBN heterostructure as it is displaced a distance d by the fiber. The top part of the figure corresponds to $d=300$ nm (strain of 5%) (c) Schematic of the strain-induced energy potential due to the fiber facet (dark blue surface). Bright (white spheres) and dark (black spheres) excitons navigate this potential through a combination of diffusion (yellow arrows) and drift (red arrow); only dark excitons have a long enough lifetime to reach the energetic minimum.

References

- [1] G. Wang, C. Robert, M. M. Glazov, F. Cadiz, E. Courtade, T. Amand, D. Lagarde, T. Taniguchi, K. Watanabe, B. Urbaszek, and X. Marie, *In-Plane Propagation of Light in Transition Metal Dichalcogenide Monolayers: Optical Selection Rules*, Phys. Rev. Lett. **119**, 047401 (2017).
- [2] X. X. Zhang, T. Cao, Z. Lu, Y. C. Lin, F. Zhang, Y. Wang, Z. Li, J. C. Hone, J. A. Robinson, D. Smirnov, S. G. Louie, and T. F. Heinz, *Magnetic brightening and control of dark excitons in monolayer WSe₂*, Nat. Nano. **12**, 883 (2017).
- [3] Y. Zhou, G. Scuri, D. S. Wild, A. A. High, A. Dibos, L. A. Jauregui, C. Shu, K. De Greve, K. Pistunova, A. Y. Joe, T. Taniguchi, K. Watanabe, P. Kim, M. D. Lukin, and H. Park, *Probing dark excitons in atomically thin semiconductors via near-field coupling to surface plasmon polaritons*, Nat. Nano. **12**, 856 (2017).
- [4] A. Branny, S. Kumar, R. Proux, and B. D. Gerardot, *Deterministic strain-induced arrays of quantum emitters in a two-dimensional semiconductor*, Nat. Commun. **8**, 15053 (2017).
- [5] C. Palacios-Berraquero, D. M. Kara, A. R. Montblanch, M. Barbone, P. Latawiec, D. Yoon, A. K. Ott, M. Loncar, A. C. Ferrari, and M. Atature, *Large-scale quantum-emitter arrays in atomically thin semiconductors*, Nat. Commun. **8**, 15093 (2017).
- [6] H. Moon, G. Grosso, C. Chakraborty, C. Peng, T. Taniguchi, K. Watanabe, and D. Englund, *Dynamic Exciton Funneling by Local Strain Control in a Monolayer Semiconductor*, Nano Lett. **20**, 6791 (2020).
- [7] M. G. Harats, J. N. Kirchhof, M. Qiao, K. Greben, and K. I. Bolotin, *Dynamics and efficient conversion of excitons to trions in non-uniformly strained monolayer WS₂*, Nat. Photonics **14**, 324 (2020).
- [8] S. Kumar, A. Kaczmarczyk, and B. D. Gerardot, *Strain-Induced Spatial and Spectral Isolation of Quantum Emitters in Mono- and Bilayer WSe₂*, Nano Lett. **15**, 7567 (2015).
- [9] W. Wu, C. K. Dass, J. R. Hendrickson, R. D. Montañó, R. E. Fischer, X. Zhang, T. H. Choudhury, J. M. Redwing, Y. Wang, and M. T. Pettes, *Locally defined quantum emission from epitaxial few-layer tungsten diselenide*, Appl. Phys. Lett. **114**, 213102 (2019).
- [10] H. Moon, E. Bersin, C. Chakraborty, A.-Y. Lu, G. Grosso, J. Kong, and D. Englund, *Strain-Correlated Localized Exciton Energy in Atomically Thin Semiconductors*, ACS Photonics **7**, 1135 (2020).
- [11] D. Lloyd, X. Liu, J. W. Christopher, L. Cantley, A. Wadehra, B. L. Kim, B. B. Goldberg, A. K. Swan, and J. S. Bunch, *Band Gap Engineering with Ultralarge Biaxial Strains in Suspended Monolayer MoS₂*, Nano Lett. **16**, 5836 (2016).
- [12] A. Falin, Q. Cai, E. J. G. Santos, D. Scullion, D. Qian, R. Zhang, Z. Yang, S. Huang, K. Watanabe, T. Taniguchi, M. R. Barnett, Y. Chen, R. S. Ruoff, and L. H. Li, *Mechanical properties of atomically thin boron nitride and the role of interlayer interactions*, Nat. Commun. **8**, 15815 (2017).
- [13] F. Cadiz, E. Courtade, C. Robert, G. Wang, Y. Shen, H. Cai, T. Taniguchi, K. Watanabe, H. Carrere, D. Lagarde, M. Manca, T. Amand, P. Renucci, S. Tongay, X. Marie, and B. Urbaszek, *Excitonic Linewidth Approaching the Homogeneous Limit in MoS₂-Based van der Waals Heterostructures*, Phys. Rev. X **7**, 021026 (2017).
- [14] G. Scuri, Y. Zhou, A. A. High, D. S. Wild, C. Shu, K. De Greve, L. A. Jauregui, T. Taniguchi, K. Watanabe, P. Kim, M. D. Lukin, and H. Park, *Large Excitonic Reflectivity of Monolayer MoSe₂ Encapsulated in Hexagonal Boron Nitride*, Phys. Rev. Lett. **120**, 037402 (2018).

- [15] K. He, N. Kumar, L. Zhao, Z. Wang, K. F. Mak, H. Zhao, and J. Shan, *Tightly bound excitons in monolayer WSe₂*, Phys. Rev. Lett. **113**, 026803 (2014).
- [16] A. V. Stier, N. P. Wilson, K. A. Velizhanin, J. Kono, X. Xu, and S. A. Crooker, *Magneto-optics of Exciton Rydberg States in a Monolayer Semiconductor*, Phys. Rev. Lett. **120**, 057405 (2018).
- [17] G. Wang, L. Bouet, D. Lagarde, M. Vidal, A. Balocchi, T. Amand, X. Marie, and B. Urbaszek, *Valley dynamics probed through charged and neutral exciton emission in monolayer WSe₂*, Phys. Rev. B **90**, 075413 (2014).
- [18] Z. Li, T. Wang, C. Jin, Z. Lu, Z. Lian, Y. Meng, M. Blei, S. Gao, T. Taniguchi, K. Watanabe, T. Ren, S. Tongay, L. Yang, D. Smirnov, T. Cao, and S. F. Shi, *Emerging photoluminescence from the dark-exciton phonon replica in monolayer WSe₂*, Nat. Commun. **10**, 2469 (2019).
- [19] E. Liu, J. van Baren, T. Taniguchi, K. Watanabe, Y.-C. Chang, and C. H. Lui, *Valley-selective chiral phonon replicas of dark excitons and trions in monolayer WSe₂*, Physical Review Research **1**, 032007(R) (2019).
- [20] S. B. Desai, G. Seol, J. S. Kang, H. Fang, C. Battaglia, R. Kapadia, J. W. Ager, J. Guo, and A. Javey, *Strain-induced indirect to direct bandgap transition in multilayer WSe₂*, Nano Lett. **14**, 4592 (2014).
- [21] O. B. Aslan, M. Deng, and T. F. Heinz, *Strain tuning of excitons in monolayer WSe₂*, Phys. Rev. B **98**, 115308 (2018).
- [22] E. Liu, J. van Baren, Z. Lu, M. M. Altairy, T. Taniguchi, K. Watanabe, D. Smirnov, and C. H. Lui, *Gate Tunable Dark Trions in Monolayer WSe₂*, Phys. Rev. Lett. **123**, 027401 (2019).
- [23] C. Robert, T. Amand, F. Cadiz, D. Lagarde, E. Courtade, M. Manca, T. Taniguchi, K. Watanabe, B. Urbaszek, and X. Marie, *Fine structure and lifetime of dark excitons in transition metal dichalcogenide monolayers*, Phys. Rev. B **96** (2017).
- [24] S. Kumar, D. Parks, and K. Kamrin, *Mechanistic Origin of the Ultrastrong Adhesion between Graphene and α -SiO₂: Beyond van der Waals*, ACS Nano **10**, 6552 (2016).
- [25] F. Cadiz, C. Robert, E. Courtade, M. Manca, L. Martinelli, T. Taniguchi, K. Watanabe, T. Amand, A. C. H. Rowe, D. Paget, B. Urbaszek, and X. Marie, *Exciton diffusion in WSe₂ monolayers embedded in a van der Waals heterostructure*, Appl. Phys. Lett. **112**, 152106 (2018).
- [26] Z. Lu, D. Rhodes, Z. Li, D. Van Tuan, Y. Jiang, J. Ludwig, Z. Jiang, Z. Lian, S.-F. Shi, J. Hone, H. Dery, and D. Smirnov, *Magnetic field mixing and splitting of bright and dark excitons in monolayer MoSe₂*, 2D Materials **7**, 015017 (2019).
- [27] L. Linhart, M. Paur, V. Smejkal, J. Burgdorfer, T. Mueller, and F. Libisch, *Localized Intervalley Defect Excitons as Single-Photon Emitters in WSe₂*, Phys. Rev. Lett. **123**, 146401 (2019).
- [28] M. M. Fogler, L. V. Butov, and K. S. Novoselov, *High-temperature superfluidity with indirect excitons in van der Waals heterostructures*, Nat. Commun. **5**, 4555 (2014).
- [29] A. A. High, J. R. Leonard, A. T. Hammack, M. M. Fogler, L. V. Butov, A. V. Kavokin, K. L. Campman, and A. C. Gossard, *Spontaneous coherence in a cold exciton gas*, Nature **483**, 584 (2012).
- [30] M. J. Burek, C. Meuwly, R. E. Evans, M. K. Bhaskar, A. Sipahigil, S. Meesala, B. Machielse, D. D. Sukachev, C. T. Nguyen, J. L. Pacheco, E. Bielejec, M. D. Lukin, and M. Loncar, *Fiber-Coupled Diamond Quantum Nanophotonic Interface*, Phys. Rev. Appl. **8**, 024026 (2017).